THE JOURNAL OF PHYSICAL CHEMISTRY B
A JOURNAL OF THE AMERICAN CHEMICAL SOCIETY

pubs.acs.org/JPCB

Article

Virus Mechanics under Molecular Crowding

Cheng Zeng, Liam Scott, Andrey Malyutin, Roya Zandi, Paul Van der Schoot, and Bogdan Dragnea*

Cite This: *J. Phys. Chem. B* 2021, 125, 1790–1798

Read Online

ACCESS | Metrics & More | Article Recommendations | Supporting Information

ABSTRACT: Viruses avoid exposure of the viral genome to harmful agents with the help of a protective protein shell known as the capsid. A secondary effect of this protective barrier is that macromolecules that may be in high concentration on the outside cannot freely diffuse across it. Therefore, inside the cell and possibly even outside, the intact virus is generally under a state of osmotic stress. Viruses deal with this type of stress in various ways. In some cases, they might harness it for infection. However, the magnitude and influence of osmotic stress on virus physical properties remains virtually unexplored for single-stranded RNA viruses—the most abundant class of viruses. Here, we report on how a model system for the positive-sense RNA icosahedral viruses, brome mosaic virus (BMV), responds to osmotic pressure. Specifically, we study the mechanical properties and structural stability of BMV under controlled molecular crowding conditions. We show that BMV is mechanically reinforced under a small external osmotic pressure but starts to yield after a threshold pressure is reached. We explain this mechanochemical behavior as an effect of the molecular crowding on the entropy of the "breathing" fluctuation modes of the virus shell. The experimental results are consistent with the viral RNA imposing a small negative internal osmotic pressure that prestresses the capsid. Our findings add a new line of inquiry to be considered when addressing the mechanisms of viral disassembly inside the crowded environment of the cell.

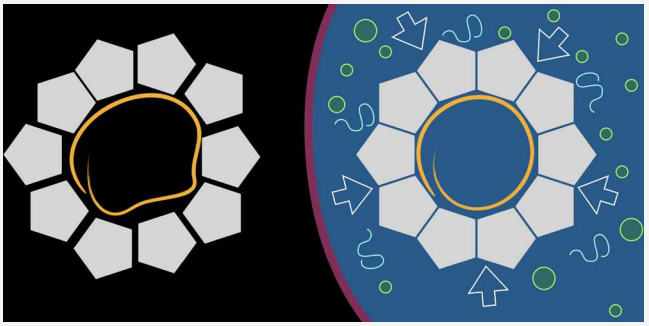

INTRODUCTION

A virus must navigate across an array of biophysical barriers that separate different chemical environments, throughout its life cycle. For instance, the pH changes as a function of the age and type of the endomembrane compartment that the virus is located in, which can trigger irreversible structural and functional transformations in the virus.[1] Another variable is the concentration of macromolecules in the cellular environment.[2] Measurements in plant cells yield osmotic pressures of 5−20 atm.[3] Exerting an osmotic pressure on a virus at entry may have important consequences for the mechanical characteristics of the particle as a whole and the properties of the protein shell subunits in particular.[4−6] The latter is often directly related to virus function,[7] including cellular entry,[8] capsid (meta)stability,[9,10] uncoating,[11] genome packaging,[12] and infectivity.[13] While the role of the osmotic stress is well established in other important biological instances of self-organization such as the beta amyloid aggregation[14] and the nucleoid structure of *Escherichia coli*,[15,16] the majority of in vitro studies on the assembly and biophysical properties of viral particles have been performed in idealized, dilute solutions. However, understanding how a virus responds to heavily crowded conditions in the interior of a cell is critical for both understanding viral life cycles and for the rational design of virus-based nanotechnologies.[17−22]

Studies have shown that macromolecular crowding affects the spherical virus assembly.[23,24] However, its influence on capsid mechanics is not clear. Specifically, the impact of osmotic pressure on the structure and mechanics of ssRNA viruses remains poorly understood. Compared with dsDNA viruses, on which the effects of osmotic pressure have been studied,[25] ssRNA viruses have a much more flexible genome. There is large bending energy penalty to be paid when packaging dsDNA in a capsid that is not paid when packaging ssRNA. Consequently, there is a large positive (outward) pressure acting in DNA viruses,[26] but not in RNA viruses.[27,28]

The flexibility of RNA and its strong interactions with the lumenal capsid interface have been predicted to result in a net pressure on the shell that is small and negative.[29−31] In other words, the electrostatic interactions between the RNA cargo and the surrounding capsid proteins actually act to pull the virus particle together. The magnitude of this negative pressure has not yet been estimated experimentally. Here, we provide such an estimate using an approach based on atomic force microscopy nanoindentation[32] of single virus particles at different osmolyte concentrations. We also show that the virus shell is mechanically reinforced under small external

Received: December 7, 2020
Revised: January 27, 2021
Published: February 12, 2021

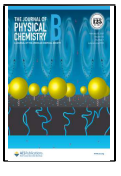

https://dx.doi.org/10.1021/acs.jpcb.0c10947
J. Phys. Chem. B 2021, 125, 1790−1798

osmotic pressures. To explain this intriguing observation, we propose a heuristic model of the capsid free energy, which includes an entropy term associated with breathing fluctuations. Mechanical property trends as a function of the osmotic pressure are qualitatively similar for empty capsids and virions but offset with respect to pressure. We associate this offset pressure value to the excess pressure on the shell due to RNA.

EXPERIMENTAL AND THEORETICAL METHODS

To study the effect of an external osmotic pressure on small ssRNA icosahedral viruses, we have chosen brome mosaic virus (BMV) as a model.[33−35] BMV is a nonenveloped virus, whose protein shell is organized with $T = 3$ icosahedral symmetry.[17] BMV has an external diameter of ≈28 nm and a segmented genome of ≈3000 nucleotides/segment.[36] Virus particles can be readily reconstituted in vitro from purified components.[37,38]

Theoretical and in vitro assembly approaches have elucidated many of the mechanistic features of BMV assembly and disassembly. It is known for instance that the genetic cargo impacts BMV assembly in multiple ways.[37,39−41] BMV virions are stabilized against disassembly at low pH (∼4.5) by strong electrostatic interactions between the capsid proteins and their genetic cargo.[42,43] To induce disassembly in vitro, these electrostatic interactions must be screened through a combination of high ionic strength (1 M LiCl), and greater than neutral pH ≳ 7. Empty capsids can be assembled at low pH and high ionic strength, that is, under conditions, which screen the electrostatic repulsion between capsid subunits occurring in the absence of genomic cargo.[44]

Similar to other positive-sense ssRNA viruses, the mechanical properties of BMV, specifically the uniaxial stress−strain and compliance characteristics, depend on the amount and type of genomic cargo.[40,45] To probe the change in mechanical compliance as a function of the osmotic pressure, we performed amplitude modulation atomic force microscopy (AFM) imaging and nanoindentation[46] experiments on BMV under controlled solution conditions, Figure 1. The buffer solutions contained the BMV native, sodium acetate−magnesium acetate (SAMA) buffer, and polyethylene glycol (PEG, MW 6000, polydispersity: 15%) as the osmolyte, at a range of final concentrations. The apparent virus elastic constant and the rupture force (Figure 2) were recorded as a function of osmotic pressure. Several other complementary approaches such as cryo-electron microscopy (cryo-EM) and dynamic scanning fluorimetry are described below.

Virus Preparation and Protein Purification. BMV was expressed in *Nicotiana benthamiana* via Agrobacterium-mediated gene delivery. The leaves were collected 7 days postinfection and stored at −80 °C until use. The leaves were first homogenized in virus buffer (250 mM NaOAc, 10 mM $MgCl_2$, pH 4.5) and then centrifuged at 5000 rpm for 25 min at 5 °C on a Beckman TA-10.250 rotor to remove undissolved materials. The supernatant was then layered on a 10% sucrose cushion (w/v) in virus buffer and centrifuged at 26,000 rpm for 3 h on a Beckman SW 32 rotor. The pellets were resuspended in 38.5% CsCl (w/v) in virus buffer and centrifuged at 45,000 rpm for 24 h on a Beckman Ti-70.1 rotor. The virus band was then collected and dialyzed, with three changes in 24 h, against SAMA buffer (50 mM NaOAc, 8 mM $Mg(OAc)_2$, pH 4.5). Final purity of wild-type virus was achieved by running the virus on a Superose-6 column by FPLC. The purified virus was dialyzed against disassembly buffer (500 mM $CaCl_2$, pH 7.4) with three changes to

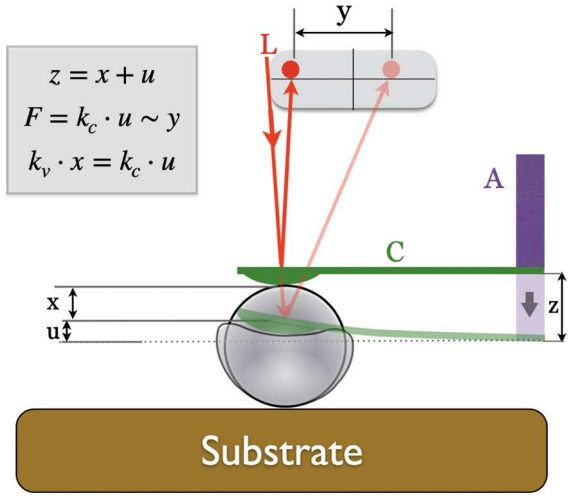

Figure 1. Cartoon of the AFM nanoindentation experiment (A: piezo-actuator, C: AFM probe cantilever, L: laser, z: actuator displacement, u: tip deflection, x: indentation depth, and y: deflection measured onto a position-sensitive detector after amplification by an optical lever). The actual indentation x due to a force F is calculated from y and z via a model of coupled springs. For an educational laboratory model and for virus nanoindentation protocols, see, e.g., refs 47 and 48, respectively.

precipitate RNA. Solution was centrifuged for 30 min at 35,000 rpm using a Beckman TLA110 rotor. The supernatant was dialyzed against Tris buffer (10 mM Tris, pH 7.4) and then TNKM buffer (50 mM tris, 50 mM NaCl, 10 mM KCl, 5 mM $MgCl_2$, pH 7.4) to produce pure protein dimers. Empty capsids were then assembled by dialyzing protein dimers in SAMA buffer with 1 M additional KCl. All samples were stored at 4 °C for the duration of the experiments.

AFM of Viral Particles. All AFM experiments were conducted with a Cypher AFM (Asylum Research) in liquid. The empty capsid sample was always examined in SAMA buffer with additional 1 M KCl, while wild-type BMV was examined in buffers both with and without 1 M additional KCl, referred to as high salt and low salt conditions, respectively. All PEG solutions are made such that they have the same salt conditions as buffers, so that mixing of PEG and buffer does not affect pH or ionic strength. For instance, a commercial 50% PEG solution and 2× SAMA buffer were mixed at 1:1 ratio to prepare a 25% PEG (w/v) stock solution in 1× SAMA buffer at pH 4.5. Ficoll solutions were prepared in the same way.

To prepare a sample for AFM, 1 μL of a stock solution of purified viral particles was first diluted in buffer and deposited onto a newly cleaved HOPG (ZYB quality, NT-MDT) surface and allowed for 10 min incubation. Half the volume of the droplet was then exchanged with fresh buffer to remove unattached virions. PEG stock solution was then added to achieve designated osmotic pressure. Another droplet of 50 μL solution was made by mixing PEG and buffer to the same PEG concentration and then used to prewet the tip. Rectangular BioLever mini tips (Olympus) with a nominal spring constant of 0.09 N/m were used in this study. The spring constant of the cantilever, k_{cant}, was calibrated according the thermal-oscillation method.[49] AFM images were acquired in AC mode with a typical imaging force below 100 pN. Viral particles were imaged closely for precise localization and particle height determination. A 1.5 nN normal force was then applied to the

https://dx.doi.org/10.1021/acs.jpcb.0c10947
J. Phys. Chem. B 2021, 125, 1790−1798

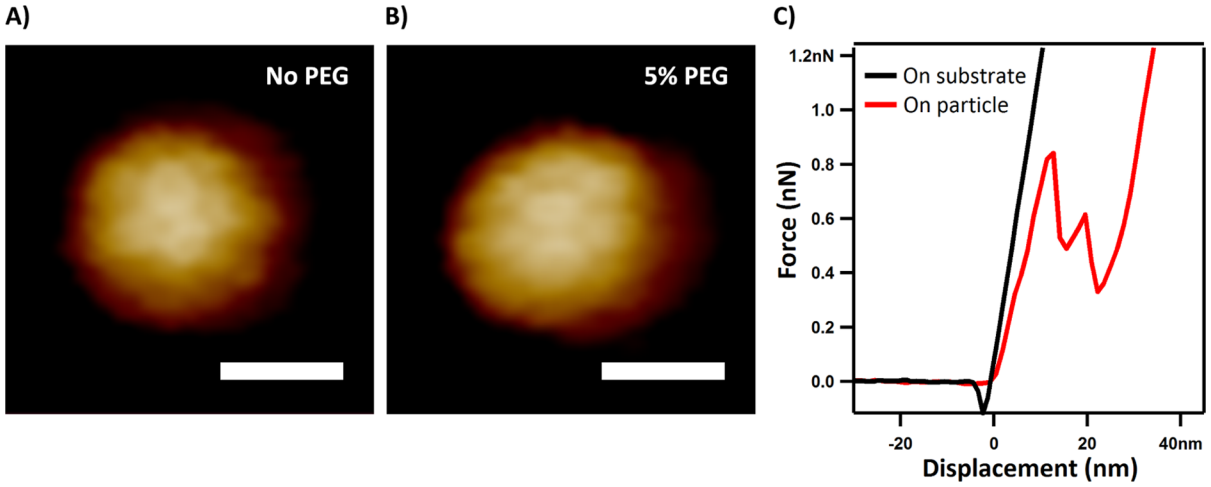

Figure 2. AFM images amplitude modulation mode in solution. (A) SAMA buffer. (B) SAMA buffer + 5% w/v PEG 6000. Scale bar: 20 nm. (C) Example of force−displacement curve acquired on a single particle (red) and on the HOPG substrate (black) used in determining the average rupture force and effective elastic constant.

center of a single particle for indentation, and a force−displacement curve was simultaneously recorded. The slope of this curve is measured by a linear fitting and defined as an effective spring constant, k_{eff}, and the vertical difference between the base line and the onset of first drastic drop in force response is defined as rupture force. By considering the virus and cantilever as two springs in series, the spring constant of the virion, k_v, can be calculated from $k_v = k_{eff} \times k_{cant}/(k_{cant} - k_{eff})$.[50]

To ensure that the force applied by the AFM tip on the sample during AC imaging was not altering the heights of the analyzed samples, an imaging force control was performed (Supporting Information Figure S4). Here, we rely on the idea that the imaging force is inversely proportional to the ratio of the tip amplitude while it is in contact with the surface and the initial amplitude of the free tip in solution. It was found that any changes in the BMV virion height due to different setpoint choices were well within the error of the experiment. The height of a virion was measured from the Z-sensor image by making a cross section through the highest point on the virion. The difference between the highest point and a reference point on the substrate was recorded as the particle height. Height histogram bin width was calculated according to Scott's rule.[51]

Differential Scanning Fluorimetry. To probe capsid structural integrity as a function of osmotic pressure, differential scanning fluorimetry (DSF) was performed in a 96-well plate using a Stratagene real-time PCR machine as described by Vaughan et al.[40] Each well had a 25 μL final volume with 4 μg virus and SYPRO orange dye at 2.5× final concentration in dimethyl sulfoxide. PEG concentrations (w/v) were controlled to be 0, 1, 2.5, 5, and 7.5%, respectively. Blank control experiments were also carried out at identical PEG and SYPRO dye concentrations under the same buffer conditions in the absence of BMV. The temperature ramp was set to be 1.0 °C/min from 25 to 95 °C. Fluorescence intensity monitored with Ex470/Em550 was recorded and plotted. The fluorescence signal from control experiments was considered as the background and subtracted from BMV fluorescence intensity. Original fluorescence intensity data were then plotted in a contour plot with respect to temperature and the PEG concentration.

Cryo-Electron Microscopy. Four microliters of sample were applied to holey carbon grids (Quantifoil 2/2, Quantifoil Micro Tools) at 6 °C and 100% RH. Grids were blotted and vitrified by plunging into liquid ethane using Vitrobot Mark III (FEI) and stored in liquid nitrogen until imaging using a JEOL JEM 3200FS operating at 300 kV. Images were acquired using a Gatan Ultrascan 4000 CCD camera under low-dose conditions (~18 $e^-/Å^2$).

Images were preprocessed using EMAN2.[52] Supervised automated particle selection of EMAN2 was used to box and extract particles from the images for single-particle reconstruction. The data sets were then processed with Auto3dEM with the initial model generated from the particle data and imposed icosahedral geometry.[53]

For size analysis, the particles were classified utilizing the Xmipp v3.1 software package. Additionally, 20 projections from the 13 Å reconstructions were produced. Classes and projections were measured in IgorPro (WaveMetrics).

Heuristic Model. To illustrate theoretically how osmotic pressure could affect shape fluctuations, the capsid was modeled as a thin elastic shell. Only the spherically symmetric, breathing mode was considered. In this highly simplified case, the entropy associated with radial fluctuations can be found analytically. The model allows the qualitative observation of changes in free energy as the osmotic pressure is varied (see Supporting Information for a detailed description). The changes in free energy are rather small on the scale of the thermal energy. This is not surprising, considering that the model only takes into consideration one type of fluctuation because it only concerns fluctuations associated with a single mode (and thus could not exceed kT anyway). More realistic, numerical simulations are on their way. However, the model illustrates the ideas that qualitatively explain our main experimental findings.

RESULTS AND DISCUSSION

PEG 6000 is a linear polymer, with a hydrodynamic radius of ≈2 nm in its collapsed state.[54] This radius is too large to allow for passive free diffusion and can thus create an osmotic pressure acting inward on the capsid. We note that the capsid still presents a finite permeability rather than zero permeability[55] but over the time scale of the experiment, we consider

https://dx.doi.org/10.1021/acs.jpcb.0c10947
J. Phys. Chem. B 2021, 125, 1790−1798

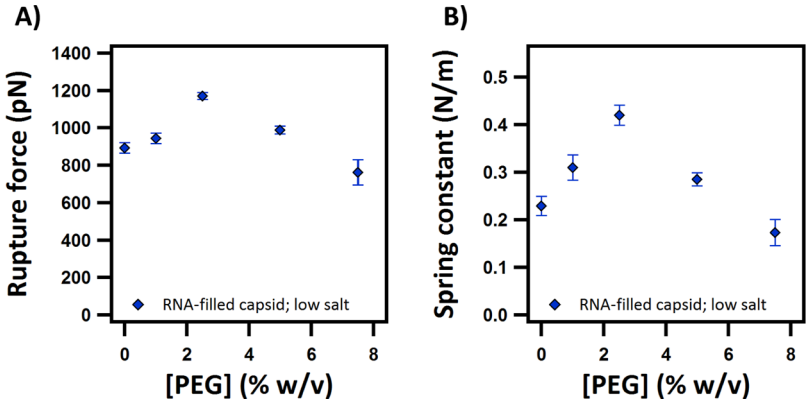

Figure 3. AFM nanoindentation results. Rupture force (A) and effective elastic constant (B) of BMV virions vs PEG concentration.

PEG 6000 diffusion across the capsid to be negligible. The concentration dependence of osmotic pressure for PEG is well documented and the polymer has been used in several studies to control osmotic pressure in biological systems[56] including bacteriophages.[25,57] It is worth noting that the viscosity of the PEG solutions[58] can be a challenge for amplitude-modulation AFM imaging. Nonetheless, in the concentration range discussed here AFM imaging in the amplitude modulation mode is possible, and topographic maps with capsomeric resolution can still be acquired, as shown in Figure 2, which shows the AFM images of single virions at 0% w/v PEG (Figure 2A) and 5% w/v PEG (Figure 2B). No structural differences, that is, loss of capsomer resolution, could be visually distinguished for particles in PEG concentrations up to the instrumental limit, which was 7.5% w/v PEG. Images across all experimental conditions can be found in the Supporting Information, Figure S1.

Changes in virion stiffness as a function of concentration were measured by AFM nanoindentation in solutions ranging from 0 to 7.5% w/v PEG. An example of force−displacement curve from a single BMV particle on a highly oriented pyrolytic graphite substrate is shown in Figure 2C. BMV displays a linear response in the limit of small applied forces.

This allows an effective spring constant for the particle to be extracted. The rupture force can also be estimated by noting the force applied at the end of the monotonical strain−stress response. Further details of how spring constant and rupture force were measured can be found in the Experimental and Theoretical section. Figure 3 shows the dependence of rupture force, stiffness, and height of wild-type (wt) BMV particles at acidic pH and low salt as a function of PEG concentration. Between 0 and 2.5% w/v, PEG the data indicate an initial increase in both rupture force and stiffness. The estimated value for the osmotic pressure because of 2.5% w/v PEG 6000 is ≈0.01 MPa, while at 7.5% w/v it reaches ≈0.1 MPa.[56] Up to this value, the particle height in our experiments remained nearly constant, within experimental error. However, at higher PEG concentrations, stiffness, rupture force, and height decrease by increasing the osmotic pressure. At low osmolyte concentrations, the effects on stiffness can be reversed by dialysis; however, at higher concentrations, virions are visibly affected for times longer than our observation time. Note that the osmotic pressure in plants (of the order of 1 MPa) is much higher than the range explored in this work. However, the virus shell is highly permeable to small solutes. Thus, the pressure range we are dealing with in this work is relevant to the osmotic pressure that a virus might experience in the cytosol, where small solutes could move freely across the shell but not nm-sized macromolecules.

To rule out the possibility that the observed behavior is induced by specific interactions between BMV and PEG instead of osmotic pressure, we performed AFM nanoindentation experiments in which PEG was substituted with a neutral, highly branched, hydrophilic polysaccharide (Ficoll, MW 70,000). As shown in Figure S2, the BMV capsid spring constant and rupture force show a similar trend with varying Ficoll concentrations. The maximum rupture force is attained at 15%w/v Ficoll. Because the Ficoll molecular weight is ≈10× that of PEG 6000 and because for an ideal solution the osmotic pressure increases linearly with molarity, we expect the osmotic pressures corresponding to the given w/v concentrations for the two osmolytes to be similar. Thus, we discard the possibility of PEG bonding to and perturbing the coat protein and retain the hypothesis of an osmotic pressure effect.

First and most striking observation is the nearly 2-fold increase in the capsid spring constant and ≈40% increase in rupture force from 0 to 2.5% w/v PEG (Figure 3). These results suggest an initial mechanical reinforcement of the viral particle by an external osmotic pressure. Intriguingly, the opposite trend is expected for fluctuating thin shells under pressure.[59] In attempting to rationalize the experimental observation of virus reinforcement, we note that the spring constant is determined by both geometric and material factors. For instance, within the assumptions of the elastic continuum theory, the spring constant for a thin spherical shell, K_v, depends on Young's modulus (E), capsid radius (R), and shell thickness (h)[60]

$$K_v \sim \frac{Eh^2}{R} \tag{1}$$

Could a geometric change, like compression of the particle diameter, explain the significant increase in K_v? To determine if the mechanical reinforcement of BMV is because of the morphological changes of the capsid, we studied it by cryo-EM with single-particle reconstruction. Figure 4 presents the single-particle reconstruction results from wtBMV in the presence of different concentrations of PEG. Figure 4A presents a side-by-side comparison of reconstructions at 0 and 5% w/v PEG, while Figure 4B shows the measured diameter of particles both from 2D classes and corresponding projections from the 3D volumes in the presence of 0% (18,500 particles), 2.5% (4600 particles), and 5% (10,000 particles) w/v PEG. Class averages and projections from these

https://dx.doi.org/10.1021/acs.jpcb.0c10947
J. Phys. Chem. B 2021, 125, 1790−1798

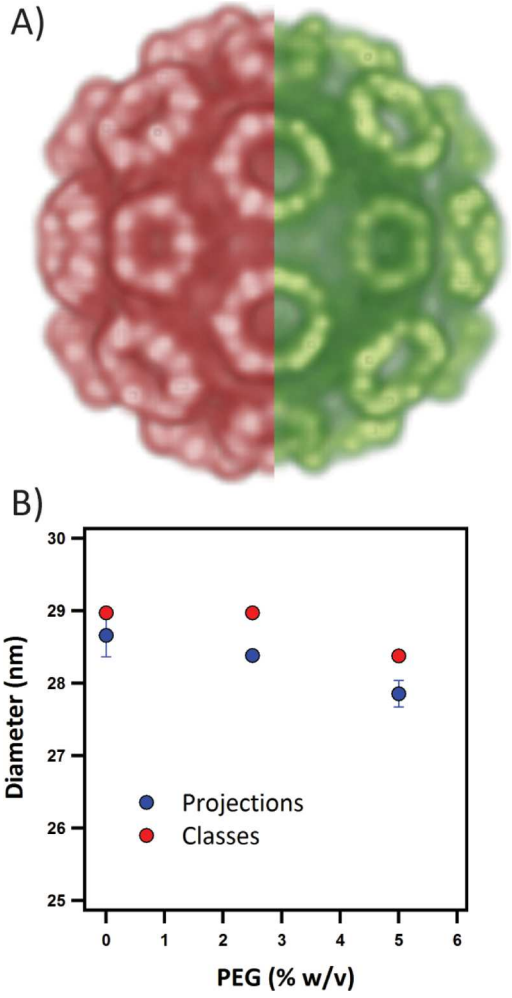

Figure 4. (A) Cryo-EM single-particle reconstruction of the wtBMV structure at 0% (red) and 5% (green) PEG. (B) BMV particle diameters of cryo-EM projections and classes as a function of PEG concentration.

experiments can be found in Figure S3. Three structures were reconstructed to approximately 13 Å resolution for each PEG concentration. Qualitatively, at this resolution, the three models were identical. Quantitatively, a comparison of the classes and projections points to a small (<1 nm) compression of the capsid upon addition of PEG. This compression appears to be limited to the protein layer, as the rings of RNA underneath the protein layer overlap perfectly in reconstructions. Because of the minimal change in diameter, a different factor than a purely geometric one must be at play.

It is well established that virus capsids undergo dynamic fluctuations at multiple scales.[61−63] Arkhipov et al. have simulated the structural dynamics of viral capsids on a microsecond timescale and found that the degree of interlocking between coat proteins determines stability of the capsids.[63] Positional fluctuations decrease interlocking at the assembly interfaces. As in fluctuating spherical shells, the elastic response to an external pressure of virus shells is expected to depend on the power spectrum of their fluctuations.[59] Osmotic pressure can reduce particle surface area-increasing fluctuations (and thus changes the fluctuation spectrum) through additional restoring depletion forces. Moreover, the increased viscosity changes the dynamics of fluctuations. Specifically, the mean-square amplitude of fluctuations per unit frequency varies inversely proportional to viscosity. Specifically, if one assumes that one subunit can be thought as a damped harmonic oscillator, according to the fluctuation−dissipation theorem, the mean-square amplitude of fluctuations is

$$\langle \Delta x^2(\omega) \rangle = \frac{k_B T}{\gamma \cdot (\omega^2 + \omega_c^2)} \quad (2)$$

where $\omega_c = \kappa/\gamma$ is the corner frequency for the elastic subunit in its pocket, that is, the frequency above which the subunit cannot respond to an external time-harmonic stimulus, and γ is the friction coefficient.[64] These qualitative arguments suggest a microscopic scenario for capsid reinforcement in which there is an interplay between positional capsomer fluctuations and osmotic pressure, Figure 5.

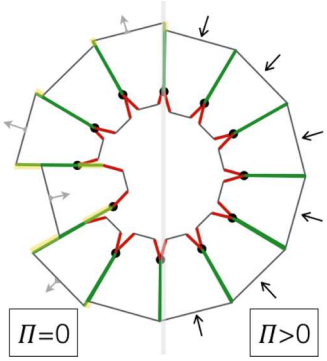

Figure 5. Cartoon of a virus shell with structural fluctuations in the absence of osmotic pressure (left half) and with fluctuations suppressed in the presence of an external osmotic pressure (right half). Assembly interfaces partially exposed because of dynamic fluctuations are highlighted in yellow (left). Pressure from an external osmolyte reduces the contour length and leads to an increase in the overlap of assembly interfaces and, thus, increased stiffness.

A simple model of the osmotic pressure compression of a spherical elastic shell with shape fluctuations was constructed along these ideas (see section "Elastic Shell with Breathing Fluctuations under Osmotic Stress" in Supporting Information). The model predicts that fluctuations are suppressed as the pressure increases. At low external pressure, the result is a drop in excess elastic free energy. This is supported by a decrease in the second moment of the deviation of the capsid radius from its average. The shell is initially rigidified by fluctuation suppression. However, once the fluctuations are stabilized further external pressure increase leads to shell compression and excess elastic energy (Supporting Information, Figure S5). This simple model captures the observed shell stabilization at low osmotic pressures, followed by destabilization as pressure is further increased. The latter is similar to predictions from fluctuation thin shells under pressure.[59]

To further test the idea of the strengthening of the capsid at intermediate osmotic pressure values, we have examined particle height distributions as a function of the PEG concentration. Particle height distributions are the result of contact mechanics, that is, they reflect the balance between elastic forces (from cohesive interactions) and adhesive forces (between virus and the substrate) occurring when virions adsorb on a surface.[65] When cohesive forces are strong relative to adhesion forces, the height is close to the diameter of the particle free in solution, but if adhesive forces are stronger, the

https://dx.doi.org/10.1021/acs.jpcb.0c10947
J. Phys. Chem. B 2021, 125, 1790−1798

particle is forced into an oblate shape and the measured height becomes smaller than the diameter. AFM has exquisite vertical resolution and the particle height can be accurately measured nonintrusively, with imaging forces below 100 pN (see control data in Supporting Information, Figure S4). Figure 6A–E shows the height distributions of wtBMV at different PEG concentrations.

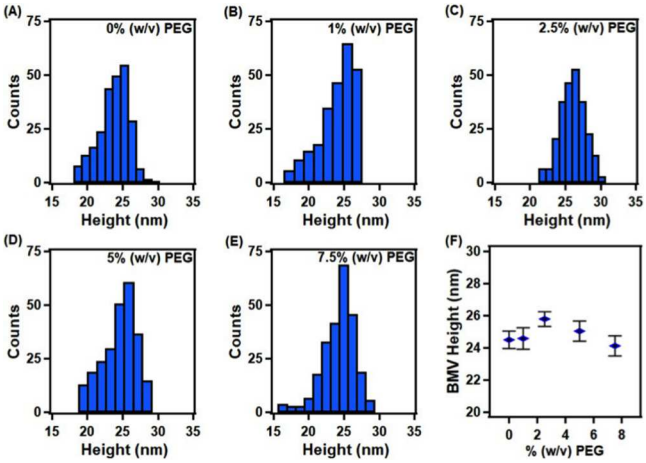

Figure 6. (A–E) Height distributions (N = 250) of wtBMV in PEG solutions at 0, 1, 2.5, 5, and 7.5%, respectively. (F) Most probable heights of BMV plotted against PEG concentration.

From height histograms, we find that the most probable particle height increases at low PEG concentrations and decreases at high PEG concentrations (Figure 6F). We attribute this increase in the particle height at 2.5% PEG to the stiffening of the virus shell. The fact that particle height is largest at 2.5% PEG concentration corroborates with nanoindentation findings, which show the stiffness of particles also peaking at this PEG concentration.

Another feature of interest in Figure 6 is the apparent asymmetry of height distributions at all concentrations but 2.5%. The extended wings at low heights suggest, again, that a larger number of particles became oblate—their cohesive forces offering reduced resistance against adhesion forces that are attempting to flatten the particles.

A more compact, less fluctuating shell would also exhibit reduced access of molecular species otherwise able to diffuse through. DSF[66] offers a convenient complementary tool to test BMV compactness under osmotic pressure. The probe undergoing diffusion in DSF is the SYPRO orange dye, which has affinity for the hydrophobic parts of proteins.[66] Thus, the measured fluorescence intensity indicates the degree of accessibility of the capsid protein's hydrophobic regions to the dye.

SYPRO dyes become fluorescent only upon binding to a hydrophobic protein patch. Because the capsid is stabilized by extended hydrophobic interactions among beta-barrel domains of CPs, we hypothesized that fluctuation suppression by osmotic pressure should make the capsomer interface less accessible to the fluorescent probe. Upon an increase in temperature, hydrophobic interactions are expected to strengthen. However, access to the protein's hydrophobic domains eventually reopens at high temperature. Figure 7 is a diagram of the fluorescence intensity as a function of PEG concentration and temperature. Individual fluorescence intensity curves were obtained with elevating temperatures at various PEG concentrations and under low salt conditions (the same as in AFM experiments). The set of DSF curves for different concentrations was transformed into a 2D contour plot.

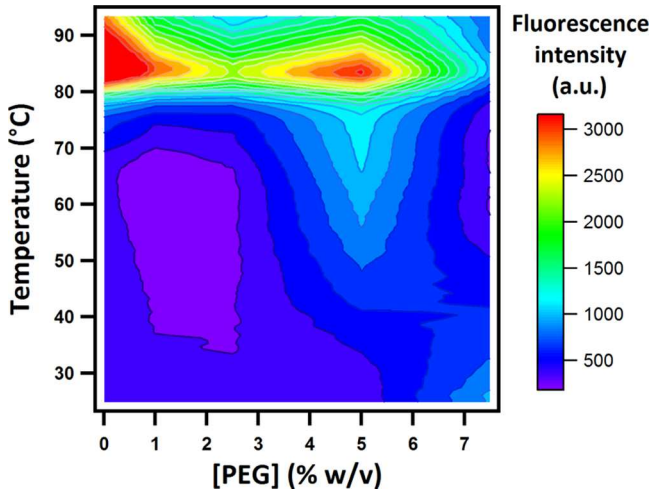

Figure 7. PEG concentration–temperature DSF diagram of wtBMV.

The temperature where the fastest increase in fluorescence intensity is observed (at ≈80 °C) is defined as the "melting" temperature of the virus capsid.[67,68] Interestingly, the major peak where melting occurs for BMV[68] does not shift when PEG is added. However, the most intriguing feature is a measurable additional suppression of fluorescence intensity between 1 and 2.5% PEG at all temperatures between 30 and 70 °C. This result can be rationalized on the same lines as those discussed above: because a freshly purified sample was used and the experiment was carried out in SAMA buffer where self-assembly is thermodynamically favored, the background fluorescence observed without PEG at room temperature should predominately come from dyes entering spaces between coat proteins, which dynamically open and close. As such, the reduction in fluorescence intensity for the 1 and 2.5% PEG samples suggests that the intercapsomer interfaces are closed by external osmotic pressure. As mentioned before, such suppression can lead to stronger interprotein interactions and is in line with the mechanical reinforcement evidence by AFM at low PEG concentrations. Thus, DSF data corroborate the AFM nanoindentation results.

At higher PEG concentrations, background fluorescence is restored, which indicates renewed access to hydrophobic protein patches. This is potentially because of compression and distortion of proteins in the virus shell. This change also suggests a microscopic mechanism for the softening of the shell at PEG concentrations beyond 2.5% found by AFM nanoindentation and imaging (Figures 3 and 6). Although the osmotic pressures involved are not large, it is known that prolonged exposure to low levels of mechanical stress can induce plastic deformations in virus capsids.[45,69]

So far, we have seen that external osmotic pressure can strengthen the capsid under certain conditions. Furthermore, simulations predict that RNA binding to the capsid lumenal interface should result in a small inward pressure.[30] Thus, there should be a potentially measurable difference between the mechanical response of empty capsids with respect to wtBMV, which is interesting to compare with the theoretical

https://dx.doi.org/10.1021/acs.jpcb.0c10947
J. Phys. Chem. B 2021, 125, 1790–1798

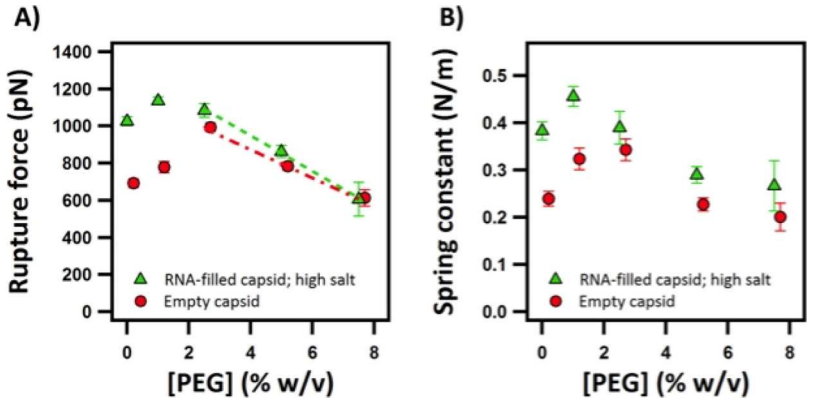

Figure 8. Comparison of rupture force and the spring constant between empty capsids and wtBMV at different PEG concentrations. The dashed lines are a guide to the eye used to find the intercept of the horizontal axis.

predictions. We studied the contribution of viral RNA to the mechanical properties of BMV through comparative AFM nanoindentation experiments on RNA-filled and empty BMV capsids at various PEG concentrations and identical buffers, Figure 8.

Empty capsids can only exist in the presence of high salt concentrations (~1 M KCl) at pH 4.5. By performing AFM nanoindentation on RNA-filled and empty BMV in the same high salt buffer, we attribute the difference in response to the effect of the ssRNA cargo. We observe: (1) the RNA-filled capsids are generally stronger than empty capsids, especially at low PEG concentrations; (2) the osmotic-pressure-induced reinforcement of RNA-filled capsids peaks at a lower PEG concentration, in comparison to their empty counterparts. Such differences can be explained by an interplay between two factors: structural differences and osmotic pressure of the RNA. Thus, from the cryo-EM data, the presence of the RNA adds approximately 1.5 nm additional thickness to the ~5 nm shell. The increase in the shell thickness could contribute to higher stiffness of the capsids, similar to previous reports on CCMV.[70] However, an effective increase in the shell thickness should lead to strengthening of the capsid regardless of the PEG concentration. Thus, the effective shell thickness difference per se is insufficient to explain the shift of the peak position. Assuming that RNA provides an internal pressure that prestresses the capsid in a similar way to PEG, we deduce wtBMV should require a smaller amount of PEG to reach the peak corresponding to the jammed state of coat proteins. The order of magnitude of this negative pressure can be inferred from the shift in the peak position. The presence of the RNA shifts the peak from 2.5 to 1% PEG, which corresponds to a difference of ≈0.01 MPa of osmotic pressure.[56] This small negative pressure due to RNA agrees with predicted values from the electrostatic models.[29,30] In support of the electrostatic origins of these observed differences, we note that the reinforcement peak of RNA-filled BMV particles at 2.5% PEG under low-salt conditions (Figure 2) shifts to 1% PEG under high-salt conditions (Figure 8). However, it should be noted that when Erdemci-Tandogan et al. theoretically considered the impact of RNA base-pairing on the stability of capsid,[31] they found that the secondary structure of RNA does play a role in the value of the negative pressure. This would be interesting to test in future experiments with RNA variants. Another question for the future opened by this research concerns the physiological role of the nonmonotonic dependence of the capsid mechanical strength on the osmotic pressure, in particular the potential implications that an increased virion stability might have for the long distance (cell-to-cell and, for BMV, through hydraulic transport throughout tissue) after entry.[71] For instance, BMV is believed to disassemble immediately after opportunistic inoculation via a wound but it has a tripartite genome that requires three different virions in the same place at the same time. Long-distance transport of intact virions and spread might occur if they are stabilized by osmotic pressure. Moreover, the results presented here raise questions about the mechanochemical effects that an extracellular milieu such as mucus in an airway tract, or the endosomal lumen might have on the virions of other viruses of broader interest.

CONCLUSIONS

We provide evidence for ssRNA icosahedral virus shells being mechanically reinforced at moderate osmotic pressures. Initially, the added osmotic pressure promotes protein−protein interactions leading to a jammed state. Thus, qualitatively, the reinforcement can be understood through a partial suppression of the inherent dynamics of the viral protein subunits. The trend of mechanical reinforcement is reversed at higher external osmotic pressure, when mechanical fatigue eventually happens. By comparing the mechanical response of empty capsids and wtBMV under osmotic stress, we found that RNA prestresses the capsid by exerting a negative pressure on the lumenal interface of the virus shell. We provided an order of magnitude estimate for this pressure contribution from RNA at ≈0.01 MPa. Overall, the results of this study highlight the significant differences in virus mechanics that may arise in a crowded, physiological environment, with potential implications for disassembly and genome presentation.

ASSOCIATED CONTENT

Supporting Information

The Supporting Information is available free of charge at https://pubs.acs.org/doi/10.1021/acs.jpcb.0c10947.

Results of control experiments (AFM and cryo-EM) and statistical theory of an elastic shell with breathing fluctuations under osmotic stress (PDF)

https://dx.doi.org/10.1021/acs.jpcb.0c10947
J. Phys. Chem. B 2021, 125, 1790−1798

AUTHOR INFORMATION

Corresponding Author

Bogdan Dragnea − *Department of Chemistry, Indiana University, Bloomington, Bloomington, Indiana 47405, United States;* orcid.org/0000-0003-0611-2006; Phone: +1 812 856 0087; Email: dragnea@indiana.edu

Authors

Cheng Zeng − *Department of Chemistry, Indiana University, Bloomington, Bloomington, Indiana 47405, United States*

Liam Scott − *Department of Chemistry, Indiana University, Bloomington, Bloomington, Indiana 47405, United States*

Andrey Malyutin − *Department of Chemistry, Indiana University, Bloomington, Bloomington, Indiana 47405, United States*

Roya Zandi − *Department of Physics and Astronomy, University of California at Riverside, Riverside, California 92521, United States;* orcid.org/0000-0001-8769-0419

Paul Van der Schoot − *Eindhoven University of Technology, 5600 MB Eindhoven, Netherlands*

Complete contact information is available at: https://pubs.acs.org/10.1021/acs.jpcb.0c10947

Notes

The authors declare no competing financial interest.

ACKNOWLEDGMENTS

R.Z. was supported by the National Science Foundation through grant no. DMR-1719550. B.D. acknowledges support by the Army Research Office, under Award W911NF-17-1-0329 and the National Science Foundation, under Award CBET 1803440. The authors are grateful to Dr. Irina Tsvetkova for support with samples and training.

REFERENCES

(1) Martinière, A.; Bassil, E.; Jublanc, E.; Alcon, C.; Reguera, M.; Sentenac, H.; Blumwald, E.; Paris, N. In vivo intracellular pH measurements in tobacco and arabidopsis reveal an unexpected pH gradient in the endomembrane system. *Plant Cell* **2013**, *25*, 4028−4043.

(2) Zimmerman, S. B.; Trach, S. O. Estimation of Macromolecule Concentrations and Excluded Volume Effects for the Cytoplasm of Escherichia-Coli. *J. Mol. Biol.* **1991**, *222*, 599−620.

(3) Bennet-Clark, T.; Greenwood, A.; Barker, J. Water Relations and Osmotic Pressures of Plant Cells. *New Phytol.* **1936**, *35*, 277.

(4) Homouz, D.; Perham, M.; Samiotakis, A.; Cheung, M. S.; Wittung-Stafshede, P. Crowded, cell-like environment induces shape changes in aspherical protein. *Proc. Natl. Acad. Sci. U.S.A.* **2008**, *105*, 11754−11759.

(5) Sarkar, M.; Smith, A. E.; Pielak, G. J. Impact of reconstituted cytosol on protein stability. *Proc. Natl. Acad. Sci. U.S.A.* **2013**, *110*, 19342−19347.

(6) Colla, T.; Bakhshandeh, A.; Levin, Y. Osmotic stress and pore nucleation in charged biological nanoshells and capsids. *Soft Matter* **2020**, *16*, 2390−2405.

(7) Greber, U. F. How cells tune viral mechanics−insights from biophysical measurements of influenza virus. *Biophys. J.* **2014**, *106*, 2317−2321.

(8) Ramalho, R.; Rankovic, S.; Zhou, J.; Aiken, C.; Rousso, I. Analysis of the mechanical properties of wild type and hyperstable mutants of the HIV-1 capsid. *Retrovirology* **2016**, *13*, 17.

(9) Bauer, D. W.; Li, D.; Huffman, J.; Homa, F. L.; Wilson, K.; Leavitt, J. C.; Casjens, S. R.; Baines, J.; Evilevitch, A. Exploring the Balance between DNA Pressure and Capsid Stability in Herpesviruses and Phages. *J. Virol.* **2015**, *89*, 9288−9298.

(10) Castellanos, M.; Pérez, R.; Carrasco, C.; Hernando-Pérez, M.; Gómez-Herrero, J.; de Pablo, P. J.; Mateu, M. G. Mechanical elasticity as a physical signature of conformational dynamics in a virus particle. *Proc. Natl. Acad. Sci. U.S.A.* **2012**, *109*, 12028−12033.

(11) Castellanos, M.; Pérez, R.; Carrillo, P. J. P.; de Pablo, P. J.; Mateu, M. G.; Pérez, R.; Carrillo, P. J. P.; de Pablo, P. J.; Mateu, M. G. Mechanical disassembly of single virus particles reveals kinetic intermediates predicted by theory. *Biophys. J.* **2012**, *102*, 2615−2624.

(12) Knobler, C. M.; Gelbart, W. M. Physical chemistry of DNA viruses. *Annu. Rev. Phys. Chem.* **2009**, *60*, 367−383.

(13) Brandariz-Nuñez, A.; Liu, T.; Du, T.; Evilevitch, A. Pressure-driven release of viral genome into a host nucleus is a mechanism leading to herpes infection. *eLife* **2019**, *8*, No. e47212.

(14) Voelker, M. J.; Urbanc, B.; Betnel, M. A Computational Study of Amyloid β-Protein Assembly in Crowded Environments. *Biophys. J.* **2015**, *108*, 525a.

(15) van der Schoot, P. Protein-Induced Collapse of Polymer Chains. *Macromolecules* **1998**, *31*, 4635−4638.

(16) de Vries, R. DNA condensation in bacteria: Interplay between macromolecular crowding and nucleoid proteins. *Biochimie* **2010**, *92*, 1715−1721.

(17) Wang, D.; Capehart, S. L.; Pal, S.; Liu, M.; Zhang, L.; Schuck, P. J.; Liu, Y.; Yan, H.; Francis, M. B.; De Yoreo, J. J. Hierarchical Assembly of Plasmonic Nanostructures Using Virus Capsid Scaffolds on DNA Origami Templates. *ACS Nano* **2014**, *8*, 7896−7904.

(18) Guenther, C. M.; Kuypers, B. E.; Lam, M. T.; Robinson, T. M.; Zhao, J.; Suh, J. Synthetic virology: Engineering viruses for gene delivery. *Wiley Interdiscip. Rev.: Nanomed. Nanobiotechnol.* **2014**, *6*, 548.

(19) Saxena, P.; Thuenemann, E. C.; Sainsbury, F.; Lomonossoff, G. P. *Recombinant Proteins from Plants: Methods and Protocols*, 2nd ed.; MacDonald, J., Kolotilin, I., Menassa, R., Eds.; Methods in Molecular Biology; Humana Press, 2016; Vol. *1385*, pp 39−54.

(20) Wörsdörfer, B.; Woycechowsky, K. J.; Hilvert, D. Directed evolution of a protein container. *Science* **2011**, *331*, 589−592.

(21) Lomonossoff, G. P.; Wege, C. *Advances in Virus Research, Vol 102*; Palukaitis, P., Roossinck, M. J., Eds.; Advances in Virus Research; Academic Press, 2018; Vol. *102*, pp 149−176.

(22) Shahgolzari, M.; Pazhouhandeh, M.; Milani, M.; Yari Khosroushahi, A.; Fiering, S. Plant viral nanoparticles for packaging and in vivo delivery of bioactive cargos. *Wiley Interdiscip. Rev.: Nanomed. Nanobiotechnol.* **2020**, *12*, No. e1629.

(23) Rincón, V.; Bocanegra, R.; Rodríguez-Huete, A.; Rivas, G.; Mateu, M. G. Effects of macromolecular crowding on the inhibition of virus assembly and virus-cell receptor recognition. *Biophys. J.* **2011**, *100*, 738−746.

(24) Smith, G. R.; Xie, L.; Lee, B.; Schwartz, R. Applying molecular crowding models to simulations of virus capsid assembly in vitro. *Biophys. J.* **2014**, *106*, 310−320.

(25) Evilevitch, A.; Lavelle, L.; Knobler, C. M.; Raspaud, E.; Gelbart, W. M. Osmotic pressure inhibition of DNA ejection from phage. *Proc. Natl. Acad. Sci. U.S.A.* **2003**, *100*, 9292−9295.

(26) Gelbart, W. M.; Knobler, C. M. VIROLOGY: Pressurized Viruses. *Science* **2009**, *323*, 1682−1683.

(27) Gopal, A.; Egecioglu, D. E.; Yoffe, A. M.; Ben-Shaul, A.; Rao, A. L. N.; Knobler, C. M.; Gelbart, W. M. Viral RNAs Are Unusually Compact. *PLoS One* **2014**, *9*, No. e105875.

(28) Zandi, R.; Dragnea, B.; Travesset, A.; Podgornik, R. On virus growth and form. *Phys. Rep.* **2020**, *847*, 1−102.

(29) Van Der Schoot, P.; Bruinsma, R. Electrostatics and the assembly of an RNA virus. *Phys. Rev. E: Stat., Nonlinear, Soft Matter Phys.* **2005**, *71*, 061928.

(30) Šiber, A.; Božič, A. L.; Podgornik, R. Energies and pressures in viruses: contribution of nonspecific electrostatic interactions. *Phys. Chem. Chem. Phys.* **2011**, *14*, 3746−3765.

(31) Erdemci-Tandogan, G.; Wagner, J.; van der Schoot, P.; Podgornik, R.; Zandi, R. Effects of RNA branching on the electrostatic stabilization of viruses. *Phys. Rev. E* **2016**, *94*, 022408.

(32) *Handbook of Nanoindentation with Biological Applications*; Oyen, M. L., Ed.; Routledge, 2010; pp 1−358.
(33) Kao, C. C.; Sivakumaran, K. Brome mosaic virus, good for an RNA virologist's basic needs. *Mol. Plant Pathol.* **2000**, *1*, 91−97.
(34) Noueiry, A. O.; Ahlquist, P. Brome mosaic virus RNA replication: revealing the role of the host in RNA virus replication. *Annu. Rev. Phytopathol.* **2003**, *41*, 77−98.
(35) Rao, A. L. N. Genome packaging by spherical plant RNA viruses. *Annu. Rev. Phytopathol.* **2006**, *44*, 61−87.
(36) Lucas, R. W.; Larson, S. B.; McPherson, A. The crystallographic structure of brome mosaic virus. *J. Mol. Biol.* **2002**, *317*, 95−108.
(37) Choi, Y. G.; Rao, A. L. N. Packaging of tobacco mosaic virus subgenomic RNAs by brome mosaic virus coat protein exhibits RNA controlled polymorphism. *Virology* **2000**, *275*, 249−257.
(38) Hiebert, E.; Bancroft, J. B.; Bracker, C. E. The assembly in vitro of some small spherical viruses, hybrid viruses, and other nucleoproteins. *Virology* **1968**, *34*, 492.
(39) Choi, Y. G.; Dreher, T. W.; Rao, A. L. N. tRNA elements mediate the assembly of an icosahedral RNA virus. *Proc. Natl. Acad. Sci. U.S.A.* **2002**, *99*, 655−660.
(40) Vaughan, R.; Tragesser, B.; Ni, P.; Ma, X.; Dragnea, B.; Kao, C. C. The tripartite virions of the brome mosaic virus have distinct physical properties that affect the timing of the infection process. *J. Virol.* **2014**, *88*, 6483−6491.
(41) Yi, G.; Vaughan, R. C.; Yarbrough, I.; Dharmaiah, S.; Kao, C. C. RNA Binding by the Brome Mosaic Virus Capsid Protein and the Regulation of Viral RNA Accumulation. *J. Mol. Biol.* **2009**, *391*, 314−326.
(42) Bruinsma, R. F.; Comas-Garcia, M.; Garmann, R. F.; Grosberg, A. Y. Equilibrium self-assembly of small RNA viruses. *Phys. Rev. E* **2016**, *93*, 032405.
(43) Garmann, R. F.; Comas-Garcia, M.; Koay, M. S. T.; Cornelissen, J. J. L. M.; Knobler, C. M.; Gelbart, W. M. Role of electrostatics in the assembly pathway of a single-stranded RNA virus. *J. Virol.* **2014**, *88*, 10472−10479.
(44) Pfeiffer, P.; Herzog, M.; Hirth, L. RNA viruses: stabilization of brome mosaic virus. *Philos. Trans. R. Soc. London, Ser. B* **1976**, *276*, 99−107.
(45) Hernando-Pérez, M.; Zeng, C.; Miguel, M. C.; Dragnea, B. Intermittency of Deformation and the Elastic Limit of an Icosahedral Virus under Compression. *ACS Nano* **2019**, *13*, 7842−7849.
(46) Marchetti, M.; Wuite, G.; Roos, W. Atomic force microscopy observation and characterization of single virions and virus-like particles by nano-indentation. *Curr. Opin. Virol.* **2016**, *18*, 82−88.
(47) Thompson, W. C.; Cattani, A. J.; Lee, O.; Ma, X.; Tsvetkova, I. B.; Dragnea, B. A Laboratory Model for Virus Particle Nano-indentation. *Biophysicist* **2020**, *1*, 5.
(48) Roos, W. H. How to perform a nanoindentation experiment on a virus. *Methods Mol. Biol.* **2011**, *783*, 251−264.
(49) Proksch, R.; Schäffer, T. E.; Cleveland, J. P.; Callahan, R. C.; Viani, M. B. Finite optical spot size and position corrections in thermal spring constant calibration. *Nanotechnology* **2004**, *15*, 1344−1350.
(50) Ivanovska, I. L.; de Pablo, P. J.; Ibarra, B.; Sgalari, G.; MacKintosh, F. C.; Carrascosa, J. L.; Schmidt, C. F.; Wuite, G. J. L. Bacteriophage capsids: tough nanoshells with complex elastic properties. *Proc. Natl. Acad. Sci. U.S.A.* **2004**, *101*, 7600−7605.
(51) Scott, D. W. On optimal and data-based histograms. *Biometrika* **1979**, *66*, 605−610.
(52) Tang, G.; Peng, L.; Baldwin, P. R.; Mann, D. S.; Jiang, W.; Rees, I.; Ludtke, S. J. EMAN2: An extensible image processing suite for electron microscopy. *J. Struct. Biol.* **2007**, *157*, 38−46.
(53) Yan, X.; Sinkovits, R. S.; Baker, T. S. AUTO3DEM-an automated and high throughput program for image reconstruction of icosahedral particles. *J. Struct. Biol.* **2007**, *157*, 73−82.
(54) Linegar, K. L.; Adeniran, A. E.; Kostko, A. F.; Anisimov, M. A. Hydrodynamic radius of polyethylene glycol in solution obtained by dynamic light scattering. *Colloid J.* **2010**, *72*, 279−281.
(55) Sleeboom, J. J. F.; Voudouris, P.; Punter, M. T. J. J. M.; Aangenendt, F. J.; Florea, D.; van der Schoot, P.; Wyss, H. M. Compression and Reswelling of Microgel Particles after an Osmotic Shock. *Phys. Rev. Lett.* **2017**, *119*, 098001.
(56) Money, N. P. Osmotic Pressure of Aqueous Polyethylene Glycols. *Plant Physiol.* **1989**, *91*, 766−769.
(57) Köster, S.; Evilevitch, A.; Jeembaeva, M.; Weitz, D. A. Influence of internal capsid pressure on viral infection by phage lambda. *Biophys. J.* **2009**, *97*, 1525−1529.
(58) Kirinčič, S.; Klofutar, C. Viscosity of aqueous solutions of poly(ethylene glycol)s at 298.15 K. *Fluid Phase Equilib.* **1999**, *155*, 311−325.
(59) Paulose, J.; Vliegenthart, G. A.; Gompper, G.; Nelson, D. R. Fluctuating shells under pressure. *Proc. Natl. Acad. Sci. U.S.A.* **2012**, *109*, 19551−19556.
(60) Landau, L.; Lifshitz, E. M. *Theory of Elasticity*, 3rd ed.; Elsevier Science: Amsterdam, 1984.
(61) Tama, F.; Brooks, C. L. Diversity and Identity of Mechanical Properties of Icosahedral Viral Capsids Studied with Elastic Network Normal Mode Analysis. *J. Mol. Biol.* **2005**, *345*, 299−314.
(62) May, E. R.; Brooks, C. L. Determination of viral capsid elastic properties from equilibrium thermal fluctuations. *Phys. Rev. Lett.* **2011**, *106*, 188101.
(63) Arkhipov, A.; Freddolino, P. L.; Schulten, K. Stability and Dynamics of Virus Capsids Described by Coarse-Grained Modeling. *Structure* **2006**, *14*, 1767−1777.
(64) Bustamante, C.; Macosko, J. C.; Wuite, G. J. L. Grabbing the cat by the tail: Manipulating molecules one by one. *Nat. Rev. Mol. Cell Biol.* **2000**, *1*, 130−136.
(65) Zeng, C.; Hernando-Pérez, M.; Dragnea, B.; Ma, X.; van der Schoot, P.; Zandi, R. Contact Mechanics of a Small Icosahedral Virus. *Phys. Rev. Lett.* **2017**, *119*, 038102.
(66) Niesen, F. H.; Berglund, H.; Vedadi, M. The use of differential scanning fluorimetry to detect ligand interactions that promote protein stability. *Nat. Protoc.* **2007**, *2*, 2212−2221.
(67) Tresset, G.; Chen, J.; Chevreuil, M.; Nhiri, N.; Jacquet, E.; Lansac, Y. Two-Dimensional Phase Transition of Viral Capsid Gives Insights into Subunit Interactions. *Phys. Rev. Appl.* **2017**, *7*, 014005.
(68) Chakravarty, A.; Reddy, V. S.; Rao, A. L. N. Unravelling the Stability and Capsid Dynamics of the Three Virions of Brome Mosaic Virus Assembled Autonomously In Vivo. *J. Virol.* **2020**, *94*, e01794-19. DOI: 10.1128/jvi.01794-19.
(69) Ortega-Esteban, A.; Condezo, G. N.; Pérez-Berná, A. J.; Chillón, M.; Flint, S. J.; Reguera, D.; San Martín, C.; de Pablo, P. J. Mechanics of Viral Chromatin Reveals the Pressurization of Human Adenovirus. *ACS Nano* **2015**, *9*, 10826−10833.
(70) Michel, J. P.; Ivanovska, I. L.; Gibbons, M. M.; Klug, W. S.; Knobler, C. M.; Wuite, G. J. L.; Schmidt, C. F. Nanoindentation studies of full and empty viral capsids and the effects of capsid protein mutations on elasticity and strength. *Proc. Natl. Acad. Sci. U.S.A.* **2006**, *103*, 6184−6189.
(71) Mise, K.; Ahlquist, P. Host-specificity restriction by bromovirus cell-to-cell movement protein occurs after initial cell-to-cell spread of infection in nonhost plants. *Virology* **1995**, *206*, 276−286.

https://dx.doi.org/10.1021/acs.jpcb.0c10947
J. Phys. Chem. B 2021, 125, 1790−1798